Detection of Oil Fire Smoke over Water in the Persian Gulf Region*

Abstract

Smoke from the recent Kuwait oil fires and the regional dust storms, collectively referred to as aerosol features, attracted enormous attention among a wide variety of scientists and environmentalists. Yet many real-time interpreters of NOAA Advanced Very High Resolution Radiometer (AVHRR) images have difficulties in consistently detecting and distinguishing these features. To identify aerosol features, automated statistical and non-statistical texture measures have been investigated. The appropriate measures were extended and successfully applied to this problem.

The difficulty in detecting aerosol features arises from two different phenomena. First, aerosol features such as dust, smoke, and fog have very similar signatures in the spectral dimension of AVHRR data. Second, these features vary widely in spectral signature over water versus land, during daytime versus night, and during summer versus winter. The newly developed algorithms take these highly dynamic parameters into account.

Texture measures under study include (1) co-occurrence matrix, (2) normalized difference histogram, and (3) two-dimensional (2D) Gabor functions. All of these texture measures are highly parametrized. An extensive sensitivity analysis was performed in order to select the optimum parameter set.

For final testing, a statistical unsupervised clustering algorithm was selected for comparison. Preliminary results have been encouraging. A summary of the results is presented.

Introduction

The detection of airborne aerosols remains a significant challenge in the processing of environmental satellite images. First, aerosols are often optically thin. As a result, the satellite sees some combination of haze and background which are difficult to separate. Second, an aerosol plume is not only semi-transparent, but its optical thickness varies along its length (Lee, 1989). Third, the appearance of the same aerosol varies greatly with different underlying backgrounds, e.g., land versus sea, desert versus vegetated land, and so on (Shenk and Curran, 1974). Fourth, the detectability of aerosols depends on the time of day of the satellite overpass. On visible images, sunglint can play an important part in aerosol identification. On infrared images, aerosol signatures, which are apparent at midday, often vanish at dusk and at night (Carlson and Benjamin, 1980).

Our focus is on darkly colored smoke such as that produced from the recent Kuwaiti oil fires. Black smoke has attracted considerable attention in recent years. Its release during a nuclear war has the potential of affecting the Earth's climate (Crutzen *et al.*, 1984). Thus, several researchers have modeled the effects of the Kuwaiti fires on local and regional radiation budgets (Browning *et al.*, 1991).

Produced only by actual combustion, as opposed to smoldering, oil smoke differs from forest fire smoke due to its high soot content (Chung and Le, 1984). On satellite images in the visible spectrum, the black appearance of oil smoke results from the smoke's high absorptivity (low reflectivity) and high optical depths (Pittock *et al.*, 1986). On satellite pictures in the infrared spectrum, oil smoke is semi-transparent. Thus, it tends to blend in with the image background (Limaye *et al.*, 1991). This characteristic difference between visible and infrared is used as the basis of our algorithms.

Data

The Advanced Very High Resolution Radiometer (AVHRR) aboard the NOAA polar-orbiting spacecraft has proven to be a useful tool to study the Kuwaiti oil fires (Limaye *et al.*, 1991). Its images come from five channels representing five wavelength intervals. Channels 1 and 2 measure reflected solar radiation. Channel 3 (near-infrared) measures both reflected solar (during the daytime) and emitted radiation. Channels 4 and 5 are located within the infrared (thermal) region.

As depicted in Figure 1, on 2 March 1991 the northwestern tip of the smoke plume contrasts well over the bright Kuwaiti land. Figure 1 is a raw channel 1 image. No smoke seems to be present over the waters of the Persian Gulf. This lack of contrast appears because the smoke, like the underlying sea surface, reflects so little solar radiation. As in channel 1, an enhancement of channel 2 (Figure 2) shows no trace of oil smoke over the dark sea surface background.

Channel 3 (near-infrared, Figure 3) shows several white spots over Kuwait. This is heat from several burning oil fields within Kuwait. These hotspots, which do not appear in the longwave infrared images (channels 4 and 5), are examples of the unique ability of channel 3 to detect tiny (much smaller than a 1-km pixel) but extremely hot features (Matson and Dozier, 1981; Lee and Tag, 1990; Robinson, 1991). Such hotspots, which often appear just upwind of a smoke plume, are extremely useful in the identification of many smoke plumes and the exact location of their origin.

N. Khazenie[1]
University Corporation for Atmospheric Research,
Boulder, CO 80301.
K. A. Richardson
Naval Research Laboratory, Monterey, CA 93943-5006

[1]Presently with Research and Data Systems Corporation, 7855 Walker Drive, Suite 460, Greenbelt, MD 20770.

*Presented at the Ninth Thematic Conference on Geologic Remote Sensing, Pasadena, California, 8-11 February 1993.

Photogrammetric Engineering & Remote Sensing,
Vol. 59, No. 8, August 1993, pp. 1271–1276.

0099-1112/93/5908–1271$03.00/0

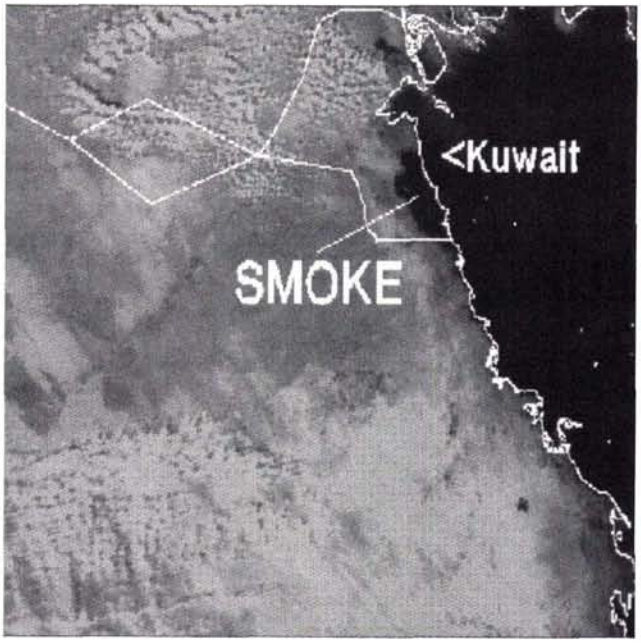

Figure 1. Channel 1, 2 March 1991.

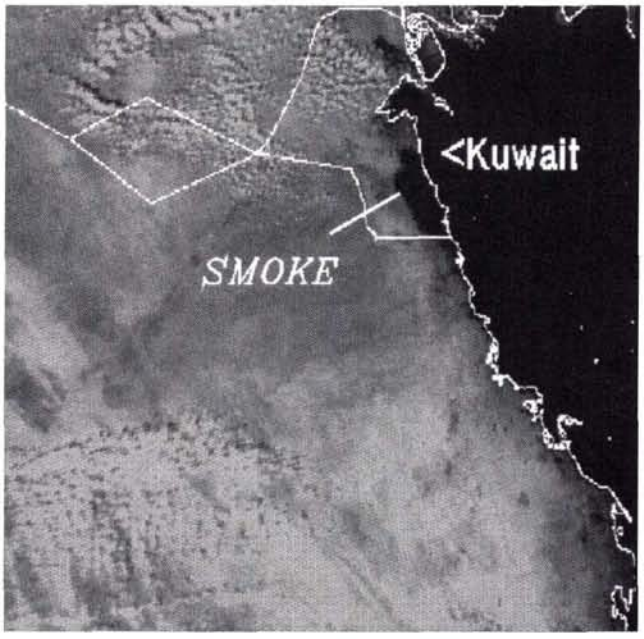

Figure 2. Channel 2, 2 March 1991.

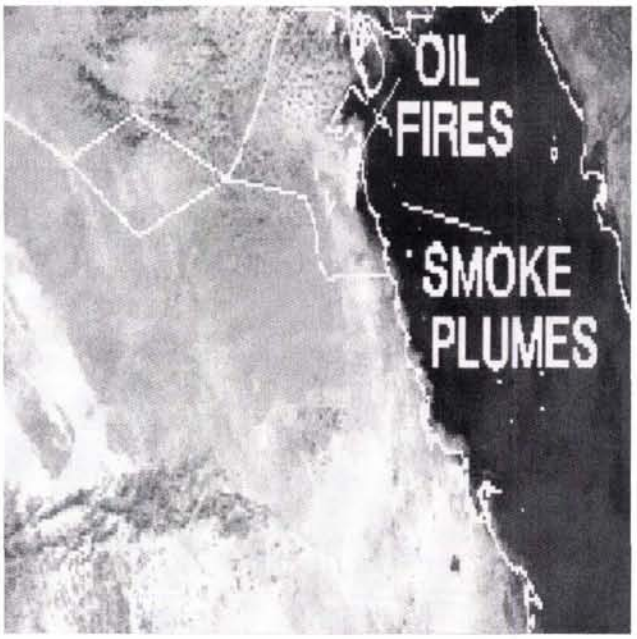

Figure 3. Channel 3, 2 March 1991.

Over the sea surface, channel 3 gives a faint view of the smoke plume. The elevated smoke appears in dark grayshades, indicating a radiative temperature lower than the background. Channel 4 (Figure 4) and channel 5 (not presented here) show smoke faintly over the Persian Gulf near the Kuwaiti coastline. The plume tends to blend with the sea surface in both of these channels farther away from the shore.

Oil smoke is nearly invisible over water on many environmental satellite images. Over land, it is visible only barely. This is due to absorption of incoming solar radiation at visible wavelengths. The raw AVHRR images by themselves show only faintly that some smoke is present.

To better understand the numerical dynamics of the raw data, several regions were selected on a related image, one taken on 28 May 1991. A histogram-equalized representation of channel 1 is shown in Figure 5. This image was selected because the oil fires have been burning for some time by this date. Oil smoke over the Gulf region was well established at this time. There is a distinct plume of smoke coming from burning wells in Kuwait as seen over land regions. However, the smoke over the Gulf is not easily observed using standard image processing enhancement techniques.

The selected regions on this image were of polygon shape. One of the polygons covered a plume of oil smoke over water, the second was ambient oil smoke over water, and the third was open water not covered by any detectable smoke. The radiances from channel 1 were processed to produce percent albedo. The resulting percent albedo values for the smoke plume range from 18 to 24 within the entire length and width of the oil smoke plume. For the oil smoke over water, the percent albedos range from 21 to 23 for selected areas. Clear waters beyond the Straits of Hormuz show more typical background percent albedo values ranging from 14 to 17. Although these are very narrow ranges, they contain the desired information.

This limited range of the radiance values, detected by the AVHRR, makes the detection of the smoke over water difficult. From the example of the 28 May 1991 scene, the clear open water translates to a range of approximately three digital counts. This is typical of clear water close to land. For the smoke over water, the digital counts are higher in the mean than for clear open water, but the range is only about

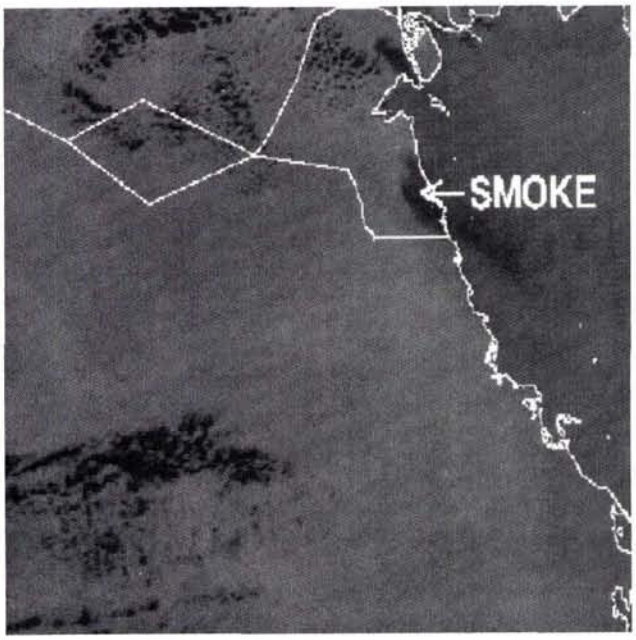

Figure 4. Channel 4, 2 March 1991.

Figure 5. Channel 1, 28 May 1991.

two digital counts. The smoke plume offers the only real signature-like variance of digital counts, with a range of approximately seven. The smoke disperses over the water to form a uniform smooth appearance much like the water itself. For typical Baysian classifiers, this does not represent much of a signature to identify with certainty. As a result, oil smoke over water is classically detectable only when the smoke is of a relatively high concentration.

In order to detect, identify, and quantify more than just the obvious plume, further processing must be undertaken. We offer a method here for processing the AVHRR data sets prior to classification. This processing provides the analysis process (the classification) with sufficient parameters to insure successful classification of the smoke features.

Methodology

The processing involves two steps. The first step, preprocessing, involves bispectral compositing. The second step involves automatic spatial textural feature discrimination.

Preprocessing

Bispectral composites of AVHRR images are first constructed to "bring out" any oil smoke signature which may be present. The composites are a ratio between AVHRR channels 1 and 2. While neither channel by itself shows any smoke over water, the ratio image often contains enough information to extract the signature.

Figure 6 shows a pixel-by-pixel ratio of channels 1 and 2. This ratio is potentially valuable in the detection of aerosols over marine areas (Haggerty *et al.*, 1990), but in its unenhanced form, shown in Figure 6, the image lacks sufficient contrast over the Persian Gulf.

Computing an image with better contrast proved difficult at first. Important detail was lost over marine regions because the ratio is subject to wide variations over land. We found most traditional enhancement techniques ineffective. Histogram equalization, for example, gave strong weight to the grayshades (smoke and non-smoke) over land, but did little to improve the contrast over the marine region.

Linear contrast stretch proved partially useful. However, this enhancement method required an inordinate amount of computing time combined with interactive human input. This made it unacceptable. We investigated a more sophisticated approach—texture analysis.

Texture Analysis

Texture measures characterize local spectral variations in an image. They are widely used for image segmentation, classification, and edge detection. Several texture measures were evaluated for their application in classification of aerosol types in AVHRR imagery. The texture measures under study included (1) Gray Level Co-Occurrence Matrix, (2) Normalized Difference Histogram, and (3) Two-Dimensional (2D) Gabor Transforms. These methods have been developed to extract textural features by means of spatial, spectral, and frequency properties of an image.

All of these texture measures produced results with different degrees of success. Gabor transforms, however, were the most efficient and robust in detecting aerosol features — especially in identifying smoke over water. Due to space limitations, we describe only the 2D Gabor family of transforms.

One of the unique properties of Gabor filters is their ability to discriminate textural features in a way similar to that of human vision (Fogel and Sagi, 1989). Another important property of the family of 2D Gabor filters is their achievement of the theoretical lower bound of joint uncertainty in the two dimensions of visual space and spatial frequency variables (Bovik *et al.*, 1990; Gabor, 1946). Other advantages in using Gabor transforms include their tunable orientation, radial frequency bandwidths, and tunable center frequencies.

The 2D Gabor filter is a harmonic oscillator, a sinusoidal

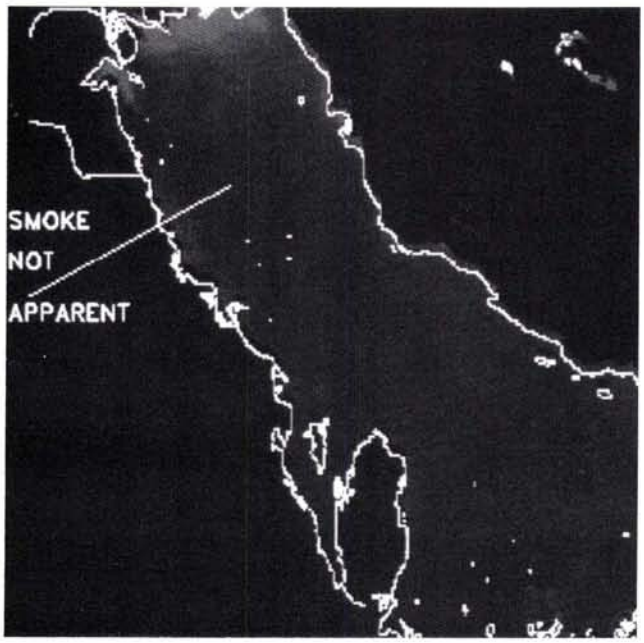

Figure 6. CH1/CH2, 2 March 1991.

plane wave within a Gaussian envelope. The convolution version of the complex 2D Gabor function has the following general form:

$$G(x,y \mid W, \theta, \varphi, X, Y) = \left(\frac{1}{2\pi\sigma^2}\right) \cdot \exp\left[\frac{-[(x-X)^2 + (y-Y)^2]}{2\sigma^2}\right] \cdot \sin(W(x\cos\theta - y\sin\theta) + \varphi). \quad (1)$$

The Gaussian width is σ, the filter orientation is θ, W is the frequency, and φ is its phase shift. Variables X and Y define the center of the filter.

The Gabor function (Equation 1) can be represented as a complex function having a real and an imaginary component, G_1 and G_2, respectively.

$$G_1(x,y \mid W, \theta, \varphi = 0, X, Y)$$

$$G_2(x,y \mid W, \theta, \varphi = \frac{\pi}{2}, X, Y)$$

Functions G_1 and G_2 are, respectively, even and odd symmetric along the preferred orientation direction θ. The results of convoluting G_1 and G_2 with any 2D function are identical except for a spectral shift of $\pi/2$ along the direction θ.

Given an image $I(x, y)$, its Gabor transformation for a given filter size n with orientation angle θ, and frequency W, is given by the following equation:

$$S^2(X,Y \mid W,\theta) = [G_1 * I(x,y)]^2 + [G_2 * I(x,y)]^2$$

In this study the response was evaluated for filters with θ = 0,° 45,° 90,° and 135.° The frequency W was $2\pi f/(n/2)$ where f = 0.5, 0.6, 0.7, 0.8, 0.9, and 1.0. The tested filter sizes n were 9, 11, 16, 32, and 64.

Results

In order to test the ability of the textural analysis to discriminate between dust, haze, and smoke, another AVHRR image was studied. This image was taken over Saudi Arabia, just south of Kuwait, on 1 March 1991. Channels 1 and 4 are shown in Figures 7 and 8, respectively. A dust storm is seen as a hook-like feature in the lower left quadrant of the figures. Some streaky haze is seen in the lower right quadrant. A faint smoke plume is seen parallel to the southern edge of the Persian Gulf. Most of the smoke is invisible over water. Note that the gray levels of the three features, dust, haze, and smoke, are practically identical here.

The ratio of channels 1 and 2 presents a very faint (nondetectable) signature of oil smoke over water. The information is there, but it cannot be seen and traditional enhancements were not effective as discussed earlier.

A total of 840 Gabor transformations were evaluated. Only one is presented here as an example. Figure 9 is the result of this transformation performed on a bispectral linear composite of channels 1 and 4 from the 1 March 1991 image. For this transformation n = 9 and θ = 45.° As this filter response indicates, the spatial textures separate the subtle differences between the three aerosol features. The dust, haze, and smoke each have distinct levels of gray.

Figure 10 illustrates the result of the texture discrimination using a Gabor transformation of the bispectral ratio composite shown in Figure 6. These spatial textures exploit the aerosol scattering properties in the shorter wavelength (channel 1) versus the longer wavelength (channel 2). In regions without smoke, channel 1 receives more reflected energy than channel 2. This suggests significant back-scattering by small, naturally occurring, airborne aerosols. Where the sea is covered by oil smoke, the reflection received by the satellite is nearly identical in the two channels. The similarity results because smoke particles tend to be relatively large, favoring increased back-scattering at the longer wavelengths.

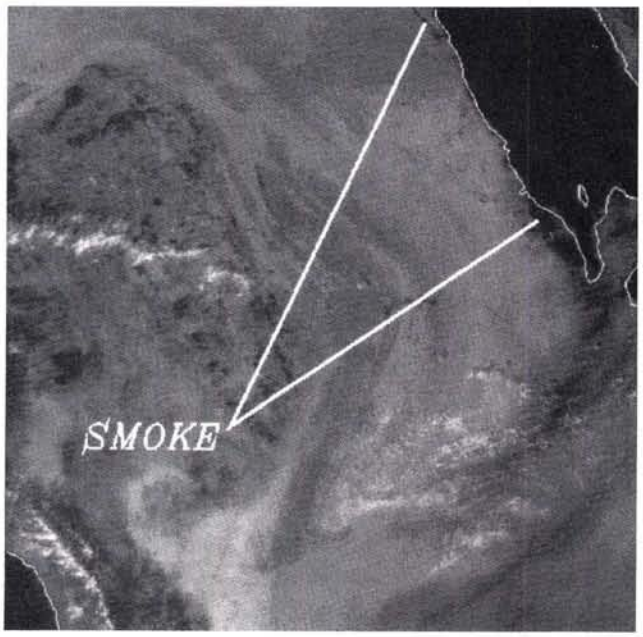

Figure 7. Channel 1, 1 March 1991.

Figure 8. Channel 4, 1 March 1991.

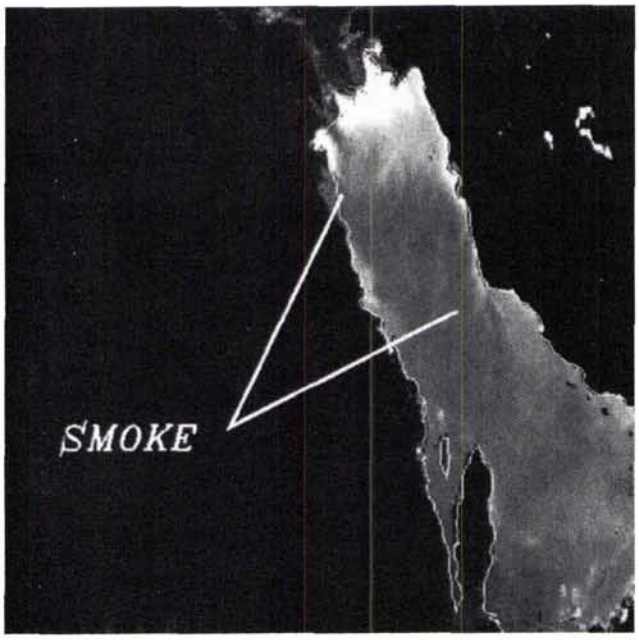

Figure 10. Texture separation, CH1/CH2, 2 March 1991.

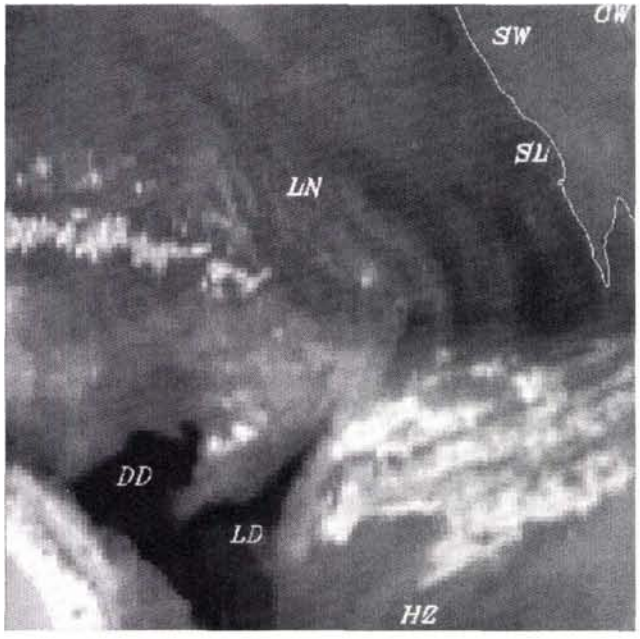

Figure 9. Gabor, $n = 9$, $\theta = 45$.

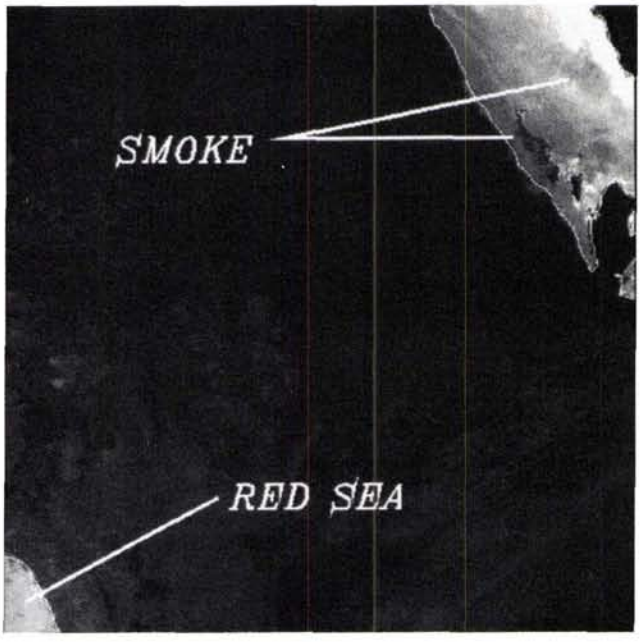

Figure 11. Texture separation, CH1/CH2, 1 March 1991.

The ratio between the channels exploits these interchannel differences and produces an improved image over the Persian Gulf. Intermediate values of the ratio (medium gray shades in Figures 10 and 11) indicate smoke over ocean. High values (nearly white areas) indicate open water.

From the 840 transforms of the 1 March 1991 image, a set of five images was selected. To this, channel 1 and 4 images were added, resulting in an image of seven bands. This image was classified to demonstrate what can be derived using the new method. A standard unsupervised statistical clustering algorithm was used. The result is shown in Figure 12. Seven clusters were identified: Land (*LN*), Deep Dust (*DD*), Light Dust (*LD*), Smoke over Water (*SW*), Smoke over Land (*SL*), Clear Water (*CW*), and Haze (*HZ*). This technique

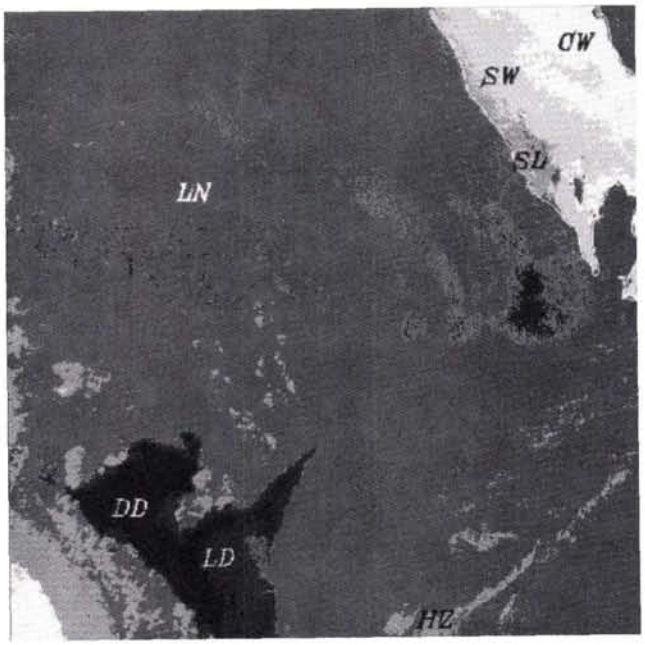

Figure 12. Clustering result, seven clusters, 1 March 1991.

Figure 13. Automatic histogram enhancement, NDVI, 28 May 1991.

was tested on several other smoke and dust images over the Persian Gulf. These images were taken at different times of the day and the results were similarly satisfactory.

To further test the method, the 28 May 1991 image was also processed. The raw channel 1, shown in Figure 5, was processed using an automatic histogram enhancement. The result, depicted in Figure 13, shows the oil smoke plume, as well as ambient smoke, covering the Gulf. The smoke is dark with the plume darkest. The smoke covers most of the Gulf nearly to the Straits of Hormuz. This was not observed using the raw images. The special processing makes the observation of the oil smoke over water possible.

Conclusion

Oil smoke produces faint, nearly invisible, signatures on satellite images. No single AVHRR channel consistently produces an easy-to-interpret image of oil smoke. The ratio image formed from channels 1 and 2 often produces dramatic improvement compared to individual channels, but will not always produce the optimal contrast between smoke and water. Innovative enhancements, such as those presented here, are needed to make the ratio image useful.

This study demonstrates a detection method which can be performed quickly and without expertise, allowing analysts to arrive at useful products in a short time. Such an approach is particularly valuable in emergency situations where users are under pressure to analyze imagery in real time. It is also instrumental in the areas of pollution control and long-term assessment of environmental impacts from aerosol plumes.

References

Bovik, A. C., M. Clark, and W. S. Geisler, 1990. Multichannel texture analysis using localized spatial filters, *IEEE Trans. on Pattern Anal. Machine Intell.*, 12(1):55–73.

Browning, K. A., R. J. Allam, S. P. Ballard, R. T. H. Barnes, D. A. Bennetts, R. H. Maryon, P. J. Mason, D. McKenna, J. F. B. Mitchell, C. A. Senior, A. Slingo, and F. B. Smith, 1991. Environmental effects from burning oil wells in Kuwait, *Nature*, 351:363–367.

Carlson, T. N., and S. G. Benjamin, 1980. Radiative heating rates for Sahara dust, *J. Atmos. Sci.*, 37:192–193.

Chung, Y. S., and H. V. Le, 1984. Detection of forest-fire smoke plumes by satellite imagery, *Atmos. Envir.*, 18:2143–2151.

Crutzen, P. J., I. E. Galbally, and C. Bruhl, 1984. Atmospheric effects of post-nuclear fires, *Climatic Change*, 6:323–364.

Fogel, I., and D. Sagi, 1989. Gabor filters as texture discriminators, *Biological Cybernetics*, 61(2):79–162.

Gabor, D., 1946. Theory of Communication, *J. IEE*, 93:429–457.

Haggerty, J., P. Derkee, and B. Wattle, 1990. A comparison of surface and satellite-based aerosol measurements in the western Mediterranean, *J. Geophys. Res.*, 95:1547–1557.

Lee, T. F., 1989. Dust tracking using composite visible/IR images— a case study, *Weather and Forecasting*, 4:258–263.

Lee, T. F., and P. M. Tag, 1990. Improved detection of hotspots using the AVHRR 3.7 μm channel, *Bull. Amer. Meteor. Soc.*, 71:1722–1730.

Limaye, S. S., V. E. Suomi, C. Velden, and G. Tripoli, 1991. Satellite observations of smoke from oil fires in Kuwait, *Science*, 252:1536–1539.

Matson, M., and J. Dozier, 1981. Identification of subresolution high temperature sources using a thermal IR sensor, *Photogrammetric Engineering & Remote Sensing*, 47:1312–1318.

Pittock, A. B., T. P. Ackerman, P. J. Crutzen, M. C. MacCracken, C. S. Shapiro, and R. P. Turco, 1986. Environmental consequences of nuclear war, *Physical and Atmospheric Effects.*, Vol. I, John Wiley and Sons, p. 358.

Robinson, J. M., 1991. Fire from space: Global fire evaluation using infrared remote sensing, *Int. J. Remote Sensing*, 12:3–24.

Shenk, W. E., and R. J. Curran, 1974. The detection of dust storms over land and water with satellite visible and infrared measurements, *Mon. Wea. Rev.*, 102:830–836.